Engineering Structures 95 (2015) 49–60

Contents lists available at ScienceDirect

Engineering Structures

journal homepage: www.elsevier.com/locate/engstruct

Shape optimization of bumper beams under high-velocity impact loads

Niyazi Tanlak [a], Fazil O. Sonmez [a,*], Mahmut Senaltun [b]

[a] Department of Mechanical Engineering, Bogazici University, Bebek 34342, Istanbul, Turkey
[b] Oyak-Renault Oto. Fab., Bursa, Turkey

ARTICLE INFO

Article history:
Received 21 August 2013
Revised 19 March 2015
Accepted 23 March 2015

Keywords:
Crashworthiness
Explicit finite element analysis
EuroNCAP
Parametric system identification
Shape optimization
Bumper beam
Spline curves

ABSTRACT

Box-shaped bumper beams mounted on vehicles serve as shock absorbers in a potential crash. In this study, their optimal shape design is investigated. The objective is to maximize the crashworthiness of the beam. The crash phenomenon in standard tests is simulated in which the vehicle hits a deformable barrier with 40% offset by 64 km/h speed. The bumper beam and the brackets supporting the beam are modeled as deformable bodies in full detail. For the rest of the car, a lumped parameter model is developed. The crash event is simulated using explicit finite element method. The design variables are the parameters defining the cross-sectional shape of the beam. The beam is optimized using a hybrid search algorithm combining Genetic and Nelder & Mead algorithms. The results indicate significant improvement in the crashworthiness of the bumper beam currently in-use. Resistance to low-velocity impact is also improved.

1. Introduction

In automotive industry, bumper beams are used as shock absorbing parts. They are attached to the front and rear ends of motor vehicles by means of brackets, which act as crash-boxes by taking the loads mainly in the axial direction. These parts need to be designed to minimize the damage to the vehicle and the risk of injury to the occupants by absorbing the energy stemming from collision. Their effectiveness under such impact loads is called crashworthiness. Better crash performance of the bumper beam reduces the effect of crash transmitted to the other components, and thereby protects them from further damage and saves the occupants from severer injury. As a design requirement, bumper beam-crash box system should absorb at least 15% of the total energy in NCAP crash tests [1]. For low velocity impact tests, on the other hand, they should absorb all the energy excluding the energy absorbed by body panel, bumper cover, reinforcement, radiator support, etc. according to the United Nations Economic Commission for Europe (ECE) Regulation No. 42. Existing bumper-beams are generally box-shaped for increased impact resistance. However, their cross-sectional profile can be modified to further improve their impact performance. This requires, first, a realistic simulation of the behavior of the bumper under crash, and then design optimization.

Although there are many studies on shape optimization of crash-boxes [1–14], the studies on beams subjected to transverse impact loads are relatively few. A number of researchers developed simulation models for bumper beams under impact conditions. Kokkula et al. [15] considered the anisotropy stemming from manufacturing processes and the effect of strain rate in the analysis of bumper beams subjected to transverse impact loads in order to obtain a realistic finite element model. They also validated the numerical model by comparing the results with the experimental data obtained by Kokkula et al. [16]. Liu and Day [17] modeled bumper beams under impact loads both numerically and analytically. In their numerical study, they neglected the frictional effects. They verified their simulation model by comparing the results with impact test data and results of an analytical model. Marzbanrad et al. [18] studied the effects of material, shape, thickness, and impact conditions on bumper-beams subjected to low-velocity impact. The materials considered in their study were aluminum, glass-mat-reinforced thermoplastics (GMT), and high strength sheet molding compound (SMC).

Some other researchers, on the other hand, conducted, besides modeling, design optimization studies to improve the performance of bumpers. Patel et al. [19] carried out topological optimization of straight and curved bumper beams subjected to static and dynamic loads using hybrid cellular automata (HCA). In the case of dynamic loading, curved beams hitting a rigid wall at 5 m/s were considered. The constitutive relation was modeled using piece-wise stress–strain curves. However, the strain rate effect was not

* Corresponding author. Tel.: +90 212 359 7196; fax: +90 212 287 2456.
E-mail address: sonmezfa@boun.edu.tr (F.O. Sonmez).

http://dx.doi.org/10.1016/j.engstruct.2015.03.046
0141-0296/

included in the model. Farkas et al. [20] found an optimal geometry for dual-channel bumper beams hitting rigid barriers at 16 km/h for offset frontal impact and at 15 km/h for pole frontal impact. Cross-sectional profile is defined using straight lines with seven geometric parameters. They created a meta-model and carried out a multi-objective optimization. Their objective was to minimize the weight and at the same time achieve force uniformity. They imposed constraints on the peak force and the largest intrusion in the bumper beam. In another study, Farkas et al. [21] considered the same problem and improved the model by including the effects of parametric uncertainties. Duponcheele and Tilley [22] conducted a topology optimization study using genetic algorithm to maximize the area moment of inertia of a bumper beam; but not considered a crash event. Zhang et al. [23] used a multi-objective formulation for optimum crash performance of rib-reinforced thin-walled hollow square beams under three-point bending drop test with a speed of 36 km/h. They used the feasible direction method as well as the ideal point method. The profile of the reinforcing rib was defined by spline curves with three variables while the outer shape is not varied. Zarei and Kroger [24] optimized the bending behavior of filled and empty hollow beams with rectangular cross section under impact loads using wall thickness and base dimensions as design variables; in other words, they optimized the size not the shape of the beam. They employed response surface methodology to build a meta-model then, using genetic algorithm, they maximized total energy absorption and specific energy absorption. They also conducted three-point bending tests under impact loading to compare the numerical and experimental results. Shin et al. [25] optimized a bumper beam together a plate connected to it with three springs. The objective was to minimize the weight using the thicknesses of these parts and the stiffnesses of the springs as variables. The constraints were pedestrian upper tibia acceleration and intrusion and deflection of the bumper beam. The plate with the springs primarily provided pedestrian protection while the bumper beam minimized the damage. Mullerschon et al. [26] carried out a topology optimization of the bumper beam based on HCA under the conditions of a mass barrier hitting the bumper beam with a velocity of 16 km/h to get uniform strain energy density. Then the resulting design was transformed into a thin-walled structure modeled with shell elements. This part was considered as having four different subsections with different thicknesses. These four thickness parameters were optimized in order to satisfy the maximum force constraint. Kim et al. [27] optimized the topology of frontal back beam reinforcement of a bumper-beam to get uniform strain energy density. They simulated full frontal and corner tests. Using response surface methodology, they created a surrogate model. Then, without changing the overall shape of the bumper beam, they varied the overall dimensions of the reinforcement to minimize the repair cost of the car, they imposed constraints on the intrusion, back beam deflection, back beam height variation.

There are also studies [28–31] that tried to minimize the risk of injury to pedestrians; but this is achieved generally by optimizing low-stiffness parts in the front of the bumper beam not the bumper beam itself, which is too rigid to have an effect in that respect.

In some of the published studies [15–18], only crash phenomena were modeled. The ones that included optimization of the bumper beam [19–23,25,26] considered the problem under low collision velocities. Only Zarei and Kroger [24] considered high collision velocities (45 km/h) under a three-point bending drop test; but they just conducted a size optimization study. The loading conditions of the bumper beams considered in the previous studies were pole frontal impact [19,23,24] and central frontal impact [25]. Moreover, the past studies mainly focused on size and thickness optimization except for a few topological [19,22] and shape [20,23] optimization studies. There is only one study [21] that modeled 40% offset impact test but with an impact velocity of 16 km/h.

All in all, the previous studies did not fully simulate the standard high-speed test conditions. One may not assume that the optimum shape designs obtained for low impact velocities are also optimum for high velocities. Although, the collision energy is not absorbed solely by the bumper beam at high collision speeds, impact energy absorbing capacity of the bumper beam will have an effect on the overall crashworthiness of the whole vehicle. Satisfaction of the requirements on the crash performance of the bumper beam for low velocity collisions is just sufficient. The effective way of optimally designing bumper beams is to maximize their crashworthiness at high speeds, thus providing the maximum protection for the passengers, while setting a constraint on their low-speed crash performance.

2. Problem statement

The types of obstacles that bumper beams endure during frontal impact are countless. Needless to say, there is an extensive literature about the collision of motor vehicles using numerous impact scenarios like [32–39]. However, they can be categorized into three major divisions: full frontal collision, offset frontal collision, and pole frontal collision. The harshest one among the three scenarios is the pole; however it is also the rarest among them. The second harshest one is the offset impact. The majority of the frontal collisions happens at an offset with varying percentages [40]. In this study, considering the severity and frequency of the three major frontal crash scenarios, the bumper beam is optimized for collisions with a 40% offset in accordance with European New Car Assessment Program (EuroNCAP), IIHS, ANCAP standard tests (See Fig. 1). The objective of this study is to develop a methodology to find the globally optimum shape or near globally optimum shapes for the cross-sectional profile of a hollow bumper beam to maximize its crash performance under the loading conditions in EuroNCAP tests.

3. Approach

3.1. The objective function

A metric is defined that is a measure of the crashworthiness of the bumper beam. Depending on the choice of the metric, different

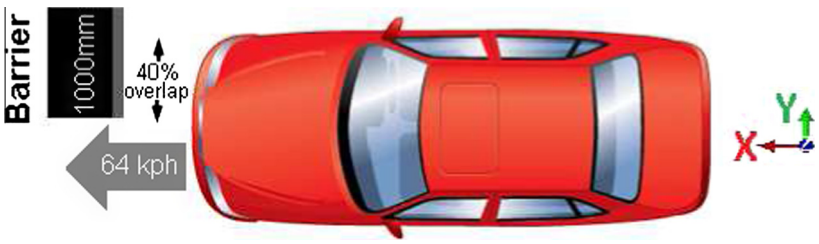

Fig. 1. A scheme for EuroNCAP Frontal offset crash tests [41].

outcomes are obtained for the optimum part design. As a measure of crash performance, the objective function to be increased is defined in this study as

$$f_{obj} = \frac{w_1}{n_1}\int_0^{t_f}\iiint_V \sigma_{ij}\dot{\epsilon}_{ij}dVdt - \frac{w_2}{n_2}\sqrt{\frac{\iiint_V(\epsilon-\bar{\epsilon})^2dV}{V}} + P \quad (1)$$

where V is the volume of the bumper beam, ϵ is the equivalent strain field, $\bar{\epsilon}$ is ϵ's mean value, t_f is the duration for which the simulation is conducted starting from initial contact with the barrier, w_i are weighting constants. The values of w_i are chosen in accordance with the relative importance that the designer gives to the individual terms; n_i are the normalization constants having values 3215 J and 600, respectively, which are the strain energy absorbed by the bumper beam currently in use and the variation in equivalent strain. These values are obtained from the offset frontal impact test simulation conducted using the bumper beam currently in use. By normalizing the terms, first the values of the terms in the objective function are ensured to be in the same range; second they have a common unit so that they can be added. The first term is the total internal energy of deformation in the bumper beam during crash. The larger the first term, the larger is the portion of the collision energy taken by the bumper. The second term is a measure of uniformity in the deformation. This term is introduced to bias the configurations in which deformation is more uniform. The smaller is this term, the more uniform is the deformation; accordingly, the integrity of the bumper – bracket system is expected to be better maintained. P is the penalty function, which includes the following terms

$$P = P_g + P_{manuf} + P_{mass} \quad (2)$$

P_g is the geometric constraint, which is activated when a cross-sectional profile selected by the search algorithm does not fit the allowable spacing. P_{manuf} is the manufacturing constraint. If the profile of the cross-section contains sharp curvatures that pose difficulties in manufacturing, P_{manuf} becomes active. The algorithm for this constraint examines the radius of curvature of the spline curve at predefined intervals to check whether there exists a segment of the profile having radius of curvature smaller than the thickness. In that case, the key-point nearest to the faulty point is replaced with two new key-points having a small specified distance in-between. Then, the curvature test is run again; if the modified spline curve passes the test, the regular procedure is followed; otherwise a high penalty value is assigned to the objective function. P_{mass} is the mass constraint such that

$$P_{mass} = \begin{cases} 0 & \text{if } m \leqslant m_{ben} \\ 1000\left(\frac{m-m_{ben}}{m_{ben}}\right)^2 + 100\left(\frac{m-m_{ben}}{m_{ben}}\right) & \text{if } m > m_{ben} \end{cases} \quad (3)$$

m is the mass of the bumper, m_{ben} is the mass of the bumper beam in current use, which is taken as a benchmark value. The constants are chosen such that the term gives small penalty values for small violations but the penalty value increases quadratically for large violations. Mass constraint is introduced in order to avoid optimal designs that show increased crashworthiness over the beam currently in use at the expense of increased weight. By adding the penalty terms to objective function, the constrained problem is transformed into an unconstrained one.

The objective of the metric above is to find the best shape of the cross-sectional profile which allows the bumper beam to absorb significant impact energy and also avoids development of extreme plastic strains leading to rupture in the bumper beam while ensuring that this is achieved without increasing the mass of the bumper beam.

3.2. Defining the shape and optimization variables

In this study, considering that bumper beam is manufactured through an extrusion process and thus cross-sectional profile is not varied along its length, only the shape of the cross-sectional profile of the bumper beam is optimized. Spline curves are used to define the profile. Accordingly, the optimization variables are the coordinates of the key points used to define the spline curves. In Fig. 2, a typical cross-section is shown. Only the frontal regions of the bumper beam are optimized, because it is fastened to the brackets having a given geometry by means of bolts from its back. As seen in the figure, the profile is defined by six key points. Five of them are free to move only in the x-direction; one of them can move in both directions. By changing the positions of the key-points, the shape of the profile is changed. During the optimization, the optimal positions of the key-points are found so that the bumper will have the highest crashworthiness according to Eq. (1).

Due to size limitations, the key points are allowed to move within a given domain. If the algorithm assigns a position for a key point outside this domain, a penalty value is added to the objective function. The spacing enclosing the current design of the bumper beam (Fig. 2) is adopted as the region within which the key points freely move.

3.3. Modeling the crash conditions

The European New Car Assessment Program (EuroNCAP) uses a deformable barrier made of aluminum honeycomb in frontal offset impact tests. The deformable barrier is designed to mimic an average collision partner during an accident.

Although quite complex structural problems can be modeled using FEM, analysis time needs to be short in design optimization studies where thousands of runs may be needed to locate the globally optimum design or a near globally optimum design. For this reason, the barrier is modeled as rigid in the simulations.

Because a rigid barrier takes none of the impact energy, the effect of collision is severer. By conducting offset frontal impact using a full car model, Deb et al. [42] showed that the results obtained using a rigid barrier with reduced vehicle speed were comparable to that of a deformable barrier with full speed. However, in this study, instead of a reduced speed, a lower mass is used for the car such that the severity of impact is more or less the same. The energy conservation equation involving collision of a vehicle with a deformable barrier can be written as

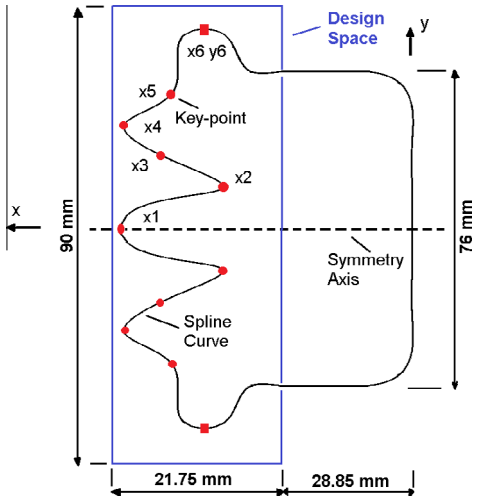

Fig. 2. Defining the cross-sectional profile of the bumper beam by spline curves described by six key points with seven variables.

$$\frac{1}{2}mv_0^2 = E_{vint} + E_{vke} + E_{bar} \tag{4}$$

where v_0 is the initial velocity of the vehicle, m is the original mass of the vehicle, E_{vint} is the energy absorbed by the vehicle, E_{vke} is the final kinetic energy of the vehicle after impact, and E_{bar} is the energy absorbed by the deformable barrier.

If the vehicle hits a rigid barrier with the same velocity, v_0, but with a different mass such that the same amount of energy, E_{vint}, is absorbed by the vehicle, then the equation becomes

$$\frac{1}{2}m'v_0^2 = E_{vint} + E'_{vke} \tag{5}$$

Here, m' is the equivalent vehicle mass and E'_{vke} is the final kinetic energy of the vehicle after impact. It now follows from Eqs. (4) and (5) that

$$m' = m - \frac{2}{v_0^2}(E_{bar} + E_{vke} - E'_{vke}) \tag{6}$$

Assuming $E_{vke} \approx E'_{vke}$ as indicated by Deb et al. [42], the above relation becomes

$$m' \approx m - \frac{2}{v_0^2}(E_{bar}) \tag{7}$$

According to Deb et al. [42], the ratio of the energy absorbed by the deformable barrier in the conventional offset test to the vehicle mass, E_{bar}/m, does not change much for cars of varying weights. Taking E_{bar}/m as 82 J/kg as suggested by Deb et al. [42], m' is found to be 0.483 m. But to be on safe side, it is taken as 0.5 m. The mass of the vehicle is 1116 kg (904 kg $+2\times 88$ kg $+36$ kg, which are the masses of Hybrid-III dummies of 88 kg and a luggage of 36 kg). So the effective mass, m', is 558 kg. Then, in the simulations a car with that mass hits a rigid wall with an initial velocity of 64 km/h (17.8 m/s) and 40% offset.

According to the simulation results of Deb et al. [42], the strain energy absorbed by the barrier is quite small compared to the energy absorbed by the vehicle during the first 10 ms of crash; only at the later stages of crash, the barrier and the vehicle absorb about the same energy. Because the barrier has a quite large stiffness compared to the bumper beam, limited deformation occurs in the barrier during the initial phases of crash and its effect on the deformation of the bumper beam is negligible as assumed in the present study. The stiffness of optimally shaped bumper beams may not be high as will be discussed later. Accordingly, the deformation in the barrier will also be limited for the optimal bumper beams. The rigid barrier assumption is considered to be valid only for the optimization of bumper beam or similar parts that are much softer than the barrier used in EuroNCAP tests and only at the initial stages of crash. If stiffer parts are to be optimized that undergo significant deformation at later stages of crash, the barrier should be modeled as deformable. Besides, it should be noted that the bumper beam is optimized for the crash event in EuroNCAP test. The beam cannot be assumed to be optimum for other crash events like pole impact, crash with a more easily deformed barrier etc.

Another concern is the modeling of the car. One option is to model the whole car as a deformable body in full detail; but this takes excessively long computational times. Considering that optimization process may require quite a number of iterations, modeling the whole car is not a feasible option.

Another alternative is to include only the bumper-bracket system in the finite element model as deformable parts and account for the inertia effects of the rest of the vehicle by two rigid mass blocks fastened to the ends of each crash-box (See Fig. 3). Although this approach is computationally effective, the accuracy of its results is questionable because no energy is absorbed by the rest of the vehicle.

In this study, knowing that these two approaches are not applicable, a lumped parameter model is developed consisting of lumped masses, springs and dampers to account for the deformation and the energy absorption behavior of the rest of the car behind the brackets.

A number of simplified models were developed by researchers to simulate the crash behavior of vehicles using dynamic system identification. The models can be classified as linear [33,43–45] or nonlinear [46,47], which may be parametric [44,45] or nonparametric [33,43,46,47]. The loadings considered in those studies were either symmetric [33,43–46] or asymmetric [43,47]. Crash phenomena were considered either at low-speed [44–46] or high-speed [33,43,45,47]. Models were tuned based on the objectives of acceleration [33,43,45], intrusion/displacement [43,44,47], force [46], energy absorption [47], and weight [43,47]. The models were either single [33,45] or multi-objective [43,44,46,47].

Fig. 4 shows a depiction of the model used in this study. The model parameters are k_1, c_1, k_{12}, c_{12}, where k_1 and c_1 denote the spring and damping effects behind the crash-boxes; while k_{12} and c_{12} denote the spring and damping effects between the different sides of the car during their relative movement. Because at the early stages of the impact plastic deformation mainly occurs in the bumper beam, then in the crash-box, after that in the remaining structural parts of the vehicle, the main body is assumed to be linearly elastic and its mechanical response can be represented by linear springs during early phases of the collision during which the simulations are continued.

In order for the lumped parameter model to represent the behavior of the car during collision, suitable values for the model parameters must be chosen. For this purpose, the results of the

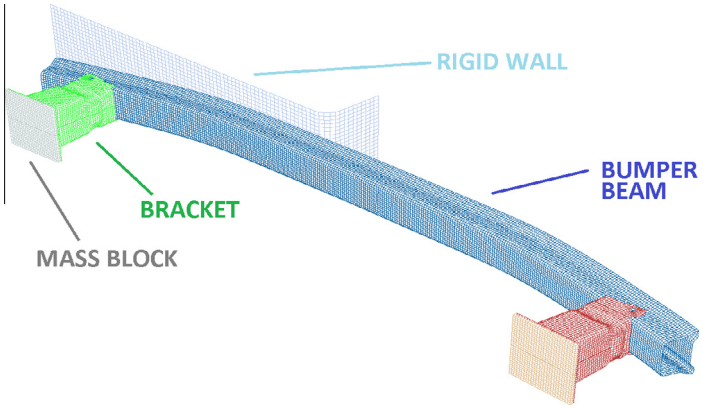

Fig. 3. The assembly of the system with mass blocks.

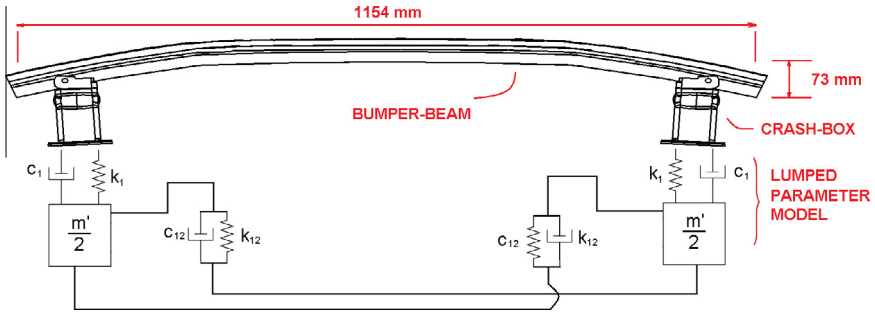

Fig. 4. A depiction of the lumped parameter model for the car structure.

present lumped parameter model of the car structure are made to match that of the full finite element model of 2010 Toyota Yaris (Sedan), which was developed and validated by The National Crash Analysis Center (NCAC) of the U.S. [48]. This car model is crashed into a rigid wall with an offset according to the scenario specified above but with a reduced speed (12.5 m/s) to account for the effect of rigid wall.

The lumped parameter model is assembled with the bumper beam and the crash-boxes as depicted in Fig. 4. The mass blocks are positioned so that the mass center of the lumped parameter model coincides with that of Yaris model. Because rotation of the vehicle occurs in the last stages of impact, rotational inertia of the vehicle is assumed not to affect the deformational behavior of the vehicle during the initial stages of impact for which simulations are conducted. Finite element simulations are conducted according to the collision scenario described above. The resulting reaction forces on the rigid wall due to the collision are calculated as a function of time. The model parameters are optimized so that the impact forces on the wall obtained using the full car model and the lumped parameter car model are as close to each other as possible. In order to judge the closeness of the two outcomes the following measure is used, which is the sum of the differences in the impact forces at corresponding time intervals.

$$f_{obj} = \sqrt{\sum_{i=0}^{100}\left[F\left(t_0 + \frac{t_f - t_0}{100}i\right) - \tilde{F}\left(t_0 + \frac{t_f - t_0}{100}i\right)\right]^2} \tag{8}$$

where t_0 is the initial time, t_f is the final time. F is the resulting impact force for Toyota Yaris model on the wall, $\tilde{F}$ is the impact force for the lumped parameter model.

The values of k_1, c_1, k_{12}, c_{12} are optimized to yield minimum f_{obj}. This optimization problem is solved using Nelder&Mead as search algorithm. As depicted in Fig. 5, the results of the lumped parameter model approximate that of the full car model. The differences may be attributed to the differences in the bumper model. The optimum values of the parameters, k_1, c_1, k_{12}, c_{12}, are found as 854.4×10^6 N/m, 193×10^3 N s/m, 609.7×10^6 N/m, 246×10^6 N s/m, respectively.

A number of lumped-parameter models with different configurations and different mass distributions are developed. The one that gives a response closest to that of the full model is chosen to be used in the design optimization. It should be also noted that the models with different mass distributions gave very similar responses especially at the initial stages of impact.

3.4. Search algorithm

After the formulation of the objective and constraint functions and definition of the optimization variables, a search algorithm is needed to find the optimum values of the variables, i.e. the optimum locations of the key-points. Considering that structural

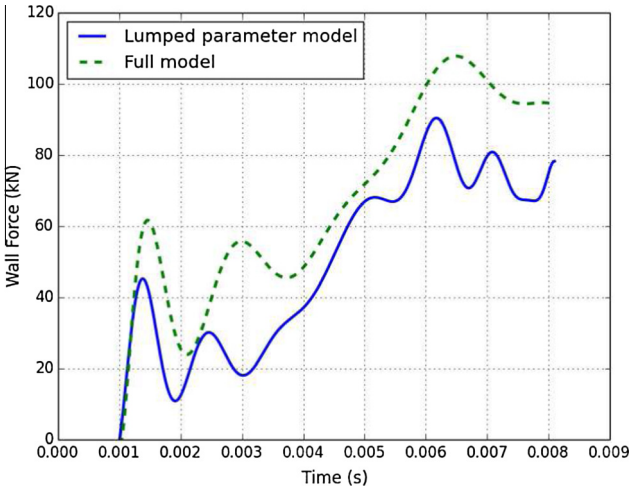

Fig. 5. Comparison of the reaction forces at the barrier resulting from car crash for the simplified lumped parameter model developed in the present study and the full finite element model provided by the National Crash Analysis Center (NCAC) [48].

optimization problems may contain numerous local optima, a local search algorithm may easily get stuck at a local optimum having a high objective function value. If the problem has a complex solution domain, multiple restarts may even not work. Heuristic global search algorithms, on the other hand, may require tens of thousands of function calls. For this reason, they are not feasible as global optimizers for problems requiring long computational times like crash simulations. Surrogate models may be developed using response surface method or artificial neural networks: but these models do not fully represent the response of the finite element analysis. In the present study, in order to search for the globally optimum design without excessive computational burden, a hybrid algorithm combining global and local search algorithms is used. In the present method, the genetic algorithm, (GA), is used to find configurations potentially close to global optimum. Then, its best results are supplied to the local optimizer, Nelder&Mead algorithm, which in turn locates the optimum. After repeating this procedure a number of times, the best result is expected to be either the global optimum or a near global optimum.

3.5. Optimization procedure

Whenever a new configuration is generated by the search algorithm, the value of the objective function for this configuration needs to be evaluated. This requires a structural analysis of the crash event to be performed. For this purpose, a FE model is developed. The FE model and the optimization algorithm are integrated using a built-in ABAQUS Python script. This code carries out FE

analyses of the configurations generated by the search algorithm, writes the results on output files, and also evaluates the results to modify the optimization variables according to the decision criteria of the hybrid search algorithm to obtain new candidate configurations.

Initially, the optimization code randomly selects values for the optimization variables within the feasible domain and creates the corresponding geometries of the bumper beam accordingly. If an initial configuration violates the manufacturing constraint, it is discarded and new random configurations are generated until a configuration satisfying this constraint is found. In this way, initial population of GA is obtained. Using the predefined velocities, boundary conditions, and the material properties, FE analyses are conducted. Based on the FE analyses, the values of the objective function are calculated.

Having completed FE analyses of the initial configurations and obtained their objective function values, the code compares these values and selects new values for the optimization variables for the next generation according to the decision criteria of the GA. This procedure is repeated until the stopping criterion is satisfied, which requires no change in the best value found in eight consecutive generations. The best points found by GA are used for creating initial simplex of Nelder&Mead algorithm. Starting from these points, Nelder&Mead tries to find the best local optimum in the neighborhood. Iterations are continued until the difference between the objective function values of the best and worst configurations becomes small.

4. Finite element modeling

Explicit FE methods are known to be better in comparison to implicit ones for structural problems involving complex contact interactions occurring within a short duration. Accordingly, commercial finite element program ABAQUS/Explicit is used in the present study to simulate the behavior of the bumper beam crash-box system during crash of the vehicle.

4.1. Initial and boundary conditions

The initial and boundary conditions defined in the FE model must reflect the conditions of the crash tests. Only in this way, the response of the bumper beam can be correctly predicted. In the present FE model, the bumper beam, crash-boxes, and the masses have an initial velocity of 64 km/h (17.8 m/s) as in the standard tests. The barrier on which the car hits is fixed; therefore its velocity is set to zero throughout the simulation.

The rear ends of the crash-boxes and the masses are constrained to move only in the direction of the initial velocity so as to prevent relative movement of the blocks in the transverse directions considering that the transverse displacements are almost zero during the initial phases of the crash as shown in Fig. 6. Rotation of the vehicle occurs only at later stages of the crash.

Because the geometry and the loading are symmetric with respect to the horizontal middle plane, only the lower portion is analyzed during the optimization process and symmetry conditions are imposed on the interface.

4.2. Analysis time

Because the crash occurs at a high velocity, the bumper beam and the crash boxes (brackets) cannot take the whole collision energy. Fig. 7 shows the strain energies of the bumper beam and the left bracket as a function of time. At the initial stages of the crash, the bumper beam takes a significant portion of the impact energy, because it has a lower stiffness than the crash-box. After about 5–6 ms, the bumper collapses like a compression spring that closes solid due to an overload; thus its resistance to further deformation significantly increases. Then, the crash box begins to take the impact energy at an increasing rate. Until about 12 ms, these parts completely collapse, their stiffness greatly increases; the other parts of the vehicle connected to the bracket, then, begin to take much of the collision energy. Considering that significant portion of the strain energy absorbed by the bumper beam before the total collapse is taken in 8 ms, the simulations are continued for 8.0 ms and the energy absorbing capacity of the bumper beam is maximized for this duration.

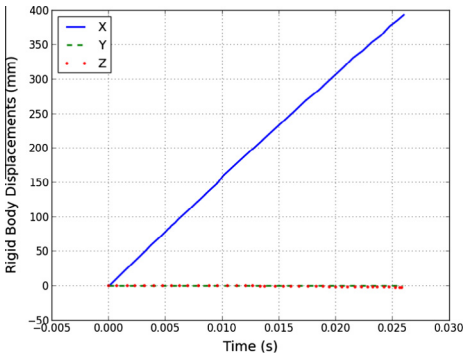

Fig. 6. Rigid body displacement history of Toyota Yaris model [48] during initial stages of offset frontal impact.

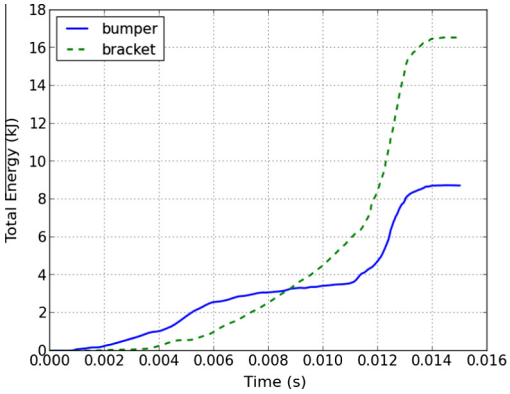

Fig. 7. Strain energies accumulated in the bumper beam currently in use and the left bracket during the collision.

4.3. Constitutive model

Materials show an increase in their yield strength with an increase in plastic strain as well as strain rate. During a crash, the bumper beam severely deforms in a very short time. For this reason, a realistic simulation of a crash event requires a constitutive equation that accounts for non-linear and strain-rate dependent deformation and also work hardening. In the present FE model, 'Johnson–Cook constitutive model [49] is used. According to this model, the equivalent flow stress of the material, $\bar{\sigma}$, depends on equivalent plastic strain and its rate, as

$$\bar{\sigma} = \left[\bar{\sigma}_0 + B(\bar{\epsilon}^{pl})^n\right]\left[1 + C\ln\left(\frac{\dot{\bar{\epsilon}}^{pl}}{\dot{\bar{\epsilon}}_0}\right)\right] \tag{9}$$

where $\bar{\epsilon}^{pl}$ is equivalent plastic strain, $\dot{\bar{\epsilon}}^{pl}$ is its rate, $\bar{\sigma}_0$ is the initial yield stress. The values of strain hardening coefficient, B, and exponent, n, can be obtained using quasi-static tension tests at constant

Table 1
The basic material properties and Johnson–Cook constants for AA6061-T6 [50].

E (GPa)	ρ (kg/m^3)	v	A (MPa)	B (MPa)	n	C	m	D_1	D_2	D_3	D_4
70	2700	0.33	324	114	0.42	0.002	1.34	−0.77	1.45	−0.47	0.0

strain rate. The value of the strain rate parameter, C, is determined through dynamic tension tests at varying strain rates. Note that temperature effect is excluded in the present model. The parameters for 6061-T6 aluminum alloy provided by Lesuer et al. [50] are given in Table 1.

4.4. Failure model

Severity of the crash may result in local failures like cracks. These may affect further deformation behavior and energy absorbing capacity of the bumper. For this reason, a cumulative failure model proposed by Johnson and Cook [51] is adopted in this study.

In the model, a critical equivalent fracture strain, $\bar{\epsilon}_f^{pl}$, is defined, which depends on hydrostatic tension, p, and effective stress, $\bar{\sigma}$. The failure strain is expressed via four material constants, D_1–D_4 (See Table 1) as

$$\bar{\epsilon}_f^{pl} = \left[D_1 + D_2 e^{D_3 \bar{\sigma}}\right]\left[1 + D_4 \ln\left(\frac{\dot{\bar{\epsilon}}^{pl}}{\dot{\epsilon}_0}\right)\right] \tag{10}$$

A damage parameter is defined as

$$\Omega = \frac{\bar{\epsilon}_0^{pl} + \sum \Delta\bar{\epsilon}^{pl}}{\bar{\epsilon}_f^{pl}} \tag{11}$$

where $\bar{\epsilon}_o^{pl}$ is the initial equivalent plastic strain and $\Delta\bar{\epsilon}^{pl}$ is an increment of the equivalent plastic strain.

As a measure of failure in finite element i, Ω_i is used, which is defined at the integration point. Failure occurs when the corresponding damage parameter, Ω_i, exceeds the unity. If failure occurs in an element, very low mechanical properties are assigned to it.

4.5. Meshing

Considering that the thickness is small in comparison to the other dimensions, shell elements are used to model the walls of the bumper beam and the brackets. The type of the element used in the model is S4R, a 4-node quadrilateral shell element with reduced integration and a large-strain formulation. The elements account for finite membrane strains and arbitrary large rotations. These elements allow transverse shear deformation. They use thick shell theory as the shell thickness increases and become discrete Kirchhoff thin shell elements as the thickness decreases. Simpson integration rule is used with five integration points through the thickness. A uniform mesh is generated in the bumper beam as shown in Fig. 3; the size of the elements is determined based on the convergence analysis.

4.6. Contact modeling

Due to severe deformation, some parts of the bumper beam and the brackets that are not initially in contact may come into contact. For this reason, the general contact algorithm, which also accounts for self-contact, is used in order to model the contact interactions in the finite element model.

4.7. Modeling of fasteners

The bumper-beam and crash-boxes are fastened by means of a bolt. Modeling the bolt in full detail poses difficulty because it has very complex geometry and it needs too many contact definitions. Therefore, a computationally effective bolt model needs to be used. For this purpose, the corresponding surfaces of the bumper-beam and bracket are connected with tie constraints without holes as explained in Tanlak et al. [52].

5. Results and discussion

5.1. Comparison of FEM results with a test case

In order to validate the accuracy of the finite element model used in the present study, the model is adapted to a similar problem and the results obtained by the FE model are compared with the experimental results. The test case is the three-point bending crash test conducted by Guo and Yu [53]. The tests as illustrated in Fig. 8 were conducted on a drop weight testing machine. The mass of the hammer was 24.23 kg and the drop height was 141.8 cm. The initial impact energy was about 336 J. The diameters of the cylindrical punch and supports were 10 mm [53].

The test is simulated using the aforementioned approach. Fig. 9 shows the relation between the force measured at the supports and the displacement measured at the middle. The numerical results correlate well with the experimental data as seen in the figure.

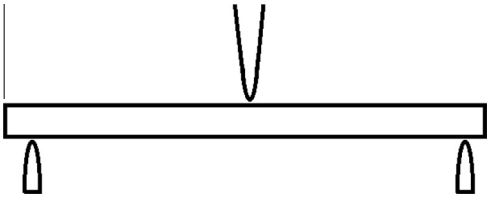

Fig. 8. A schematic of the set-up for the dynamic three-point bending tests conducted by Guo and Yu [53].

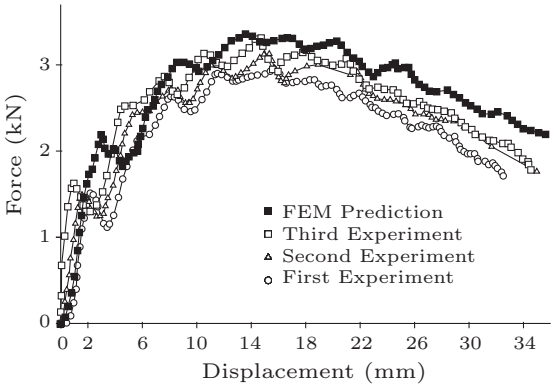

Fig. 9. Comparison of present FEM results with the three-point bending impact test data [53].

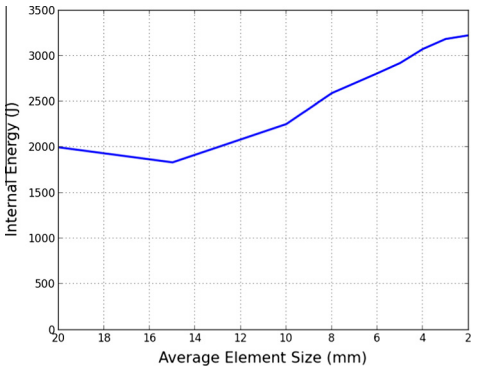

Fig. 10. Accumulated internal energies of the bumper beam for different element sizes.

5.2. Convergence analysis

Since the finite element method is an approximate solution technique, one should ensure that the resulting error is less than an acceptable limit. One of the ways to check the accuracy of the results is the mesh-convergence analysis. One should determine the range of values for the mesh size for which consistent results are obtained. The internal energy stored in the bumper is chosen as the control parameter in the convergence analysis. Fig. 10 indicates that the results converge to a value of about 3.2 kJ and 4 mm element size yields sufficiently accurate results.

5.3. Results

The shape optimization problem is solved for various combinations of weighting factors, w_i, in Eq. (1). The optimal values of the optimization variables are given in Table 2. The optimal shapes obtained by the algorithm and the chosen benchmark shapes are shown in Fig. 11 and a comparison of the results is given in Table 3.

5.4. Discussion

It is noteworthy that the mass constraint ($m \leqslant 2.03$ kg) does not become active in the optimal shapes. In all the optimal shapes, the mass is less than that of the bumper-beam currently in use. In contrast, if one tried to increase static strength of the beam, given the spacing limitations, one would introduce deeper ribs that would increase the area moment of inertia, which would in turn increase the bending strength. On the other hand, this would also increase its rigidity and thus reduce its capacity to absorb the impact energy. In that case, the rest of the vehicle, which is represented by the lumped parameter model in the present study, would take a significant portion of the impact energy. Too flexible beams, on the other hand, would quickly collapse. One should recognize that simple rules of thumb will not work in complex problems. The optimization algorithm finds the optimal shapes that cannot be intuitively known because of the complexity of the deformation behavior.

The optimal shaped beam that can absorb the largest strain energy is obtained using $w_1 = 1$ and $w_2 = 0$; i.e. by considering only the first term of the objective function. If only the second term is optimized, that means if the variance in the deformation is minimized ($w_1 = 0$ and $w_2 = 1$), the algorithm introduces deeper ribs to obtain more uniform deformation as seen in Fig. 11; but the resulting shape performs poorly in absorbing impact energy. When the two terms are considered with $w_1 = 0.8$ and $w_2 = 0.2$, an interim shape is obtained (Fig. 11).

Table 2
Optimal values of the optimization variables defining the longitudinal profile in mm.

	x_1	x_2	x_3	x_4	x_5	x_6	y_6
$w_{1,2} = 1, 0$	36.702	38.327	42.590	42.509	47.814	38.281	37.362
$w_{1,2} = 0, 1$	33.972	41.033	37.642	46.075	43.734	34.713	40.8563
$w_{1,2} = 0.8, 0.2$	36.122	40.721	43.012	41.364	47.825	40.238	36.797

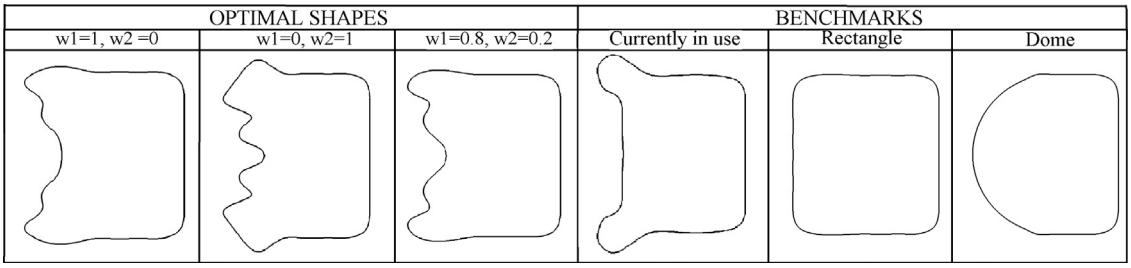

Fig. 11. Optimal profile shapes (left three) obtained using different weighting factors and benchmark shapes (right three).

Table 3
Comparison of the optimal and benchmark shapes.

	Accumulated energy (J)	Variance	Mass (kg)	Specific energy (J/kg)	Peak force (kN)	Load uniformity
Optimal shapes						
$w_{1,2} = 1, 0$	3441.9	666.2	1.88	1830.8	76.2	2.11
$w_{1,2} = 0, 1$	2209.4	329.1	1.97	1121.5	82.9	2.78
$w_{1,2} = 0.8, 0.2$	3418.2	621.8	1.91	1789.6	79.6	2.25
Bench-marks						
Currently-in-use	3215.3	599.9	2.03	1583.9	88.0	2.47
Rectangle	3165.0	844.1	1.79	1768.2	76.2	2.25
Dome	2581.6	662.4	1.63	1583.8	86.0	2.73

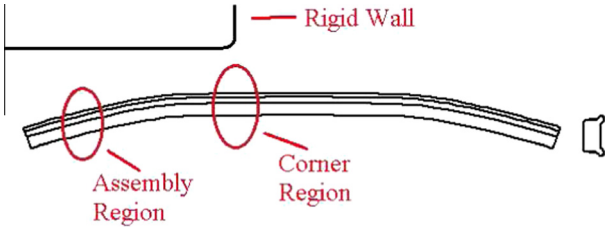

Fig. 12. The critical regions in the bumper-beam.

Benchmark beams show poorer performance in terms of both energy absorbing capacity and specific energy. Among the benchmark cases, the beam with the rectangular cross-section is the best in terms of specific energy absorbing capacity; but the total energy absorbing capacity of the beam currently in use is slightly better than that of the rectangular one.

In the bumper beam, there are two critical regions, namely the region where the bumper beam is attached to the bracket (assembly region) and the region where the contact with the rigid wall ends (corner region) as shown in Fig. 12. In the latter, a plastic hinge develops in poorly performing beams. Plastic hinge begins to form almost at the moment the car hits the wall; then the beam makes a rotation around the hinge. This occurs in beams having lower flexural stiffness like rectangular or dome-shaped beams (See Fig. 13). Poor performance of these beams may partly be attributed to the formation of plastic hinge. As seen in Fig. 13, the top three designs, which are the optimized ones, do not develop a plastic hinge.

Fig. 14 shows the shapes of the cross-sectional profiles in the two critical regions at various time intervals. Except for the stiff beam with minimum variance in deformation ($w_1 = 0$ and $w_2 = 1$), all of the beams totally collapse at the assembly region. Low stiffness beams, rectangle and dome, partially collapse in the region contacting the corner of the wall and there a plastic hinge develops.

There are other criteria that may need to be considered in bumper beam design. One such parameter is the peak force, which is largest force at the end of the crash-box. The transmitted force can be considered as a measure of the acceleration endured by the occupants. Another is the load uniformity parameter, which is defined as the peak force divided by the mean force. In order to calculate these parameters, simulations are continued until the transmitted force makes a clear descent. Among the optimized configurations, the one optimized with $w_{1,2} = 0,1$ performs best according to these criteria. It is also better than the benchmark designs. The change in the transmitted force for this design is shown in Fig. 15. These criteria may also be included in the optimization process, either in the objective function or as constraint functions; but optimization time would be longer.

Optimum design of the bumper beam for high-speed collisions increases the crashworthiness of the vehicle, thus provides increased protection for passengers; but the bumper beams should sustain limited deformation under low-speed collisions, thus prevent damage to the remaining parts of the vehicle. This requirement could be integrated to the optimization process as a constraint. However, because additional simulations would significantly increase computational times, low-velocity requirements are not considered during optimization process. Nevertheless after obtaining the optimal shapes, they are checked whether they satisfy these requirements. For this purpose three standard tests are used: the United Nations Economic Commission for Europe (ECE) Regulation No. 42, the Research Council for Automobile Repairs (RCAR) 40% offset frontal impact test, and RCAR full frontal impact test. The results of the simulations are presented in Table 4.

In the pendulum test, a pendulum having a mass equivalent to the car's mass hits the car with velocity of 4 km/h. The smaller is the permanent deformation, the better is the crash performance. In the RCAR offset frontal test, the car with a velocity of 16 km/h hits a rigid wall with an offset. In this test, the damage to the other parts of the car should be minimal; but due to the lack of data, the absorbed energies are compared. In the RCAR full frontal test, the car hits a curved rigid wall with a velocity of 10 km/h, and the intrusion, which is defined as the difference between the displacements of the middle foremost point of the bumper beam and the back end of the crash-box, and the deflection, which is defined as the difference between the displacements of the middle back side of the bumper beam and the back end of the crash-box, are measured. Table 4 shows that the two configurations obtained using $w_{1,2} = 1,0$ and $w_{1,2} = 0.8,0.2$ are better for every single criteria than the one currently in-use and better for almost all criteria for the other two benchmark shapes. So, it can be said that optimally designing the bumper beam for the EuroNCAP offset frontal impact test results in a bumper beam design that is also resistant to crashes at low speeds.

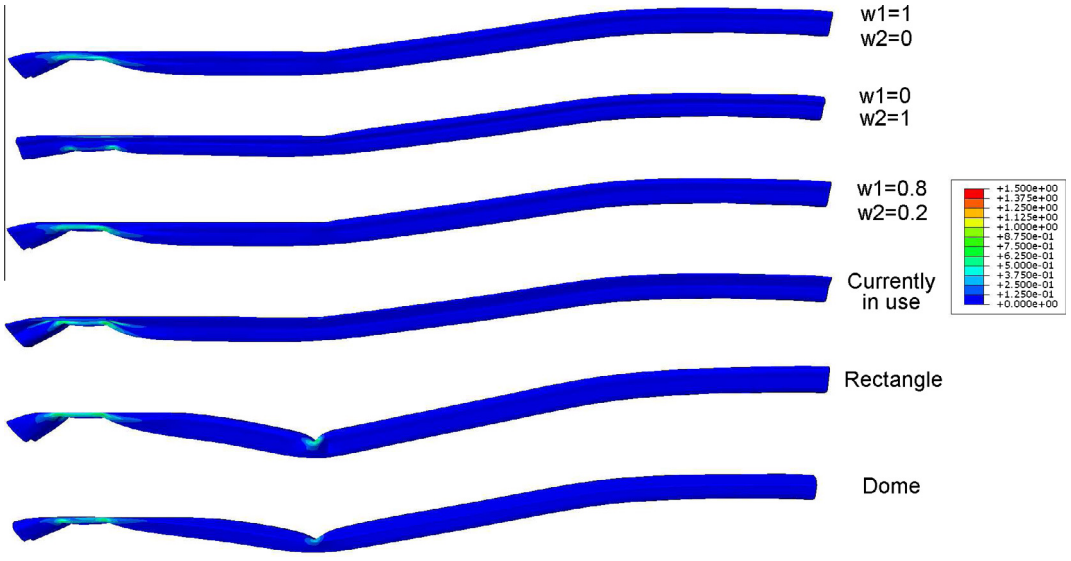

Fig. 13. Equivalent plastic strain contour plots of bumper-beam designs after 8 ms.

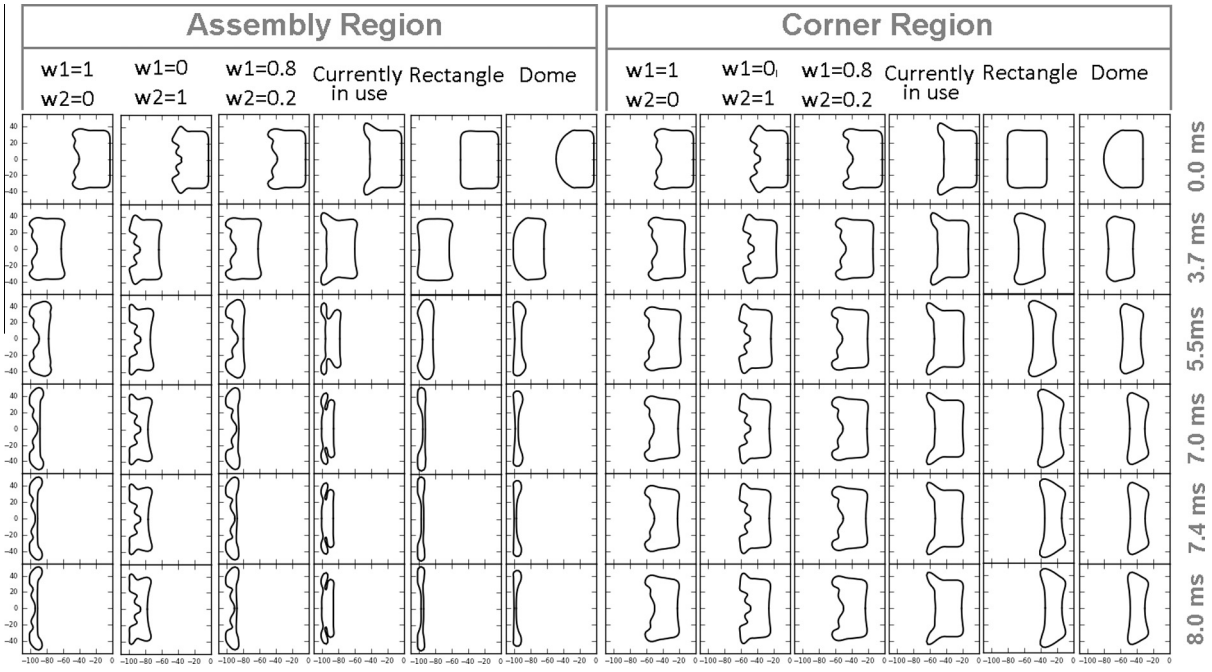

Fig. 14. The change in the shapes of cross-sections of the assembly (left six) and corner region (right six) during crash.

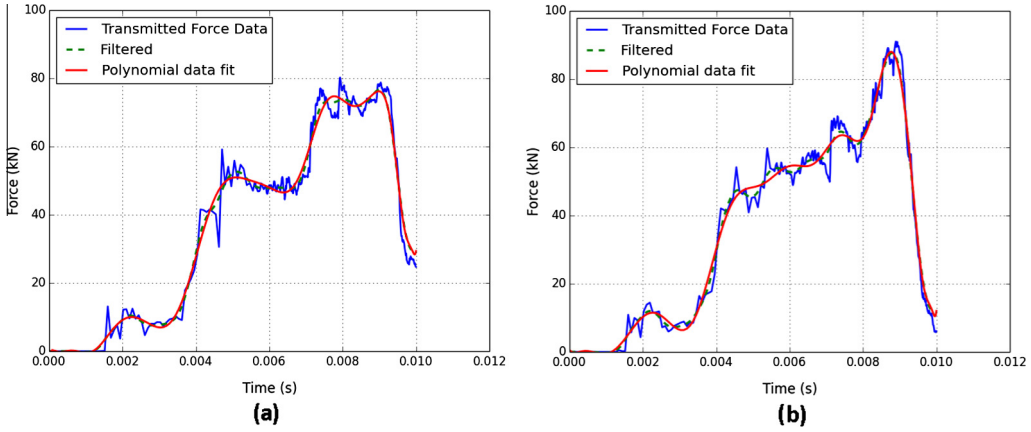

Fig. 15. The change in the transmitted force at the end of the crash-box (a) for the design optimized with $w_{1,2} = 1, 0$ and (b) for currently-in-use.

Table 4
Simulation results for low-velocity impact tests.

	Pendulum	RCAR Offset Test		RCAR Full Test	
	Plastically dissipated energy (J)	Accumulated energy (J)	Variance	Intrusion (mm)	Deflection (mm)
Optimal shapes					
w1 = 1, w2 = 0	113.1	2823.2	752	1.735	90.175
w1 = 0, w2 = 1	120.7	1586.9	934	1.242	83.421
w1 = 0.8, w2 = 0.2	111.8	2786.2	813	1.783	89.102
Bench-marks					
Currently in use	115.2	2418.7	1040	2.363	95.515
Rectangle	129	2823.5	617	24.368	138.029
Dome	141.6	2017.5	400	1.731	85.079

6. Conclusion

In the present study, the shape of a bumper beam is optimized under impact conditions very similar to EuroNCAP tests to maximize its crashworthiness. The coordinates of the key points used to define the spline curves representing the cross-sectional profile were taken as the optimization variables. The deformable barrier used in the standard tests is modeled as rigid. In order to account for the energy absorbed by the deformable barrier, a correction factor is calculated for the mass of the vehicle. Bumper beam and brackets are modeled as deformable bodies in full detail. In order to reduce the computational time, a lumped parameter model is developed to mimic the behavior of the main vehicle body using a parametric system identification method. The parameters of the simplified car model are tuned to reflect the response of the car predicted by a full car model. The resulting optimum shape found by the optimization algorithm depends highly on the formulation of the objective function, the number of variables, and the range of the feasible domain. By choosing different values for the weighting factors of the terms in the objective function, different optimal shapes are obtained. The two optimum shapes obtained in this study show significant improvement over the one currently in-use; specific strain energy absorbed by the optimal beam is larger by 16%. The resistance to crash at low speeds is also significantly improved.

Acknowledgement

Oyak-Renault Automobile and Scientific Research Projects of Bogazici University (Code number 5893) are gratefully acknowledged for supporting this research.

References

[1] Yamazaki K, Han J. Maximization of the crushing energy absorption of tubes. Struct Optim 1998;16:37–46.
[2] Hanssen AG, Langseth M, Hopperstad OS. Optimum design for energy absorption of square aluminium columns with aluminium foam filler. Int J Mech Sci 2001;43:153–76.
[3] Lee S-H, Kim H-Y, Oh S-I. Cylindrical tube optimization using response surface method based on stochastic process. J Mater Process Technol 2002;130–131:490–6.
[4] Kim CH, Arora Jasbir S. Development of simplified dynamic models using optimization: application to crushed tubes. Comput Methods Appl Mech Eng 2003;192:2073–97.
[5] Avalle M, Chiandussi G. Optimisation of a vehicle energy absorbing steel component with experimental validation. Int J Impact Eng 2007;34:843–58.
[6] Hou S, Li Q, Long S, Yang X, Li W. Design optimization of regular hexagonal thin-walled columns with crashworthiness criteria. Finite Elem Anal Des 2007;43:555–65.
[7] Liu Y. Optimum design of straight thin-walled box section beams for crashworthiness analysis. Finite Elem Anal Des 2008;44:139–47.
[8] Zarei HR, Kröger M. Optimization of the foam-filled aluminum tubes for crush box application. Thin-Wall Struct 2008;46:214–21.
[9] Acar E, Guler MA, Gerceker B, Cerit ME, Bayram B. Multi-objective crashworthiness optimization of tapered thin-walled tubes with axisymmetric indentations. Thin-Wall Struct 2011;49(1):94–105.
[10] Qi C, Yang S, Dong F. Crushing analysis and multiobjective crashworthiness optimization of tapered square tube under oblique impact loading. Thin-Wall Struct 2012;59:103–19.
[11] Yang S, Qi C. Multiobjective optimization for empty and foam-filled square columns under oblique impact loading. Int J Impact Eng 2013;54:177–91.
[12] Tanlak N, Sonmez FO. Optimal shape design of thin-walled tubes under high-velocity axial impact loads. Thin-Wall Struct 2014;84:302–12.
[13] Sun G, Song X, Baek S, Li Q. Robust optimization of foam-filled thin-walled structure based on sequential Kriging metamodel. Struct Multidisc Optim 2014;49:897–913.
[14] Li Fangyi, Sun Guangyong, Huang Xiaodong, Rong Jianhua, Li Qing. Multiobjective robust optimization for crashworthiness design of foam filled thin-walled structures with random and interval uncertainties. Eng Struct 2015;88:111–24.
[15] Kokkula S, Hopperstad OS, Lademo OG, Berstad T. Offset impact behaviour of bumper beam-longitudinal systems: numerical simulations. Int J Crash 2006;11(4):317–36.
[16] Kokkula S, Langseth M, Hopperstad OS, Lademo OG. Offset impact behaviour of bumper beam-longitudinal systems: experimental investigations. Int J Crash 2006;11(4):299–316.
[17] Liu Y, Day ML. Experimental analysis and computer simulation of automotive bumper system under impact conditions. Int J Comput Methods Eng Sci Mech 2008;9:51–9.
[18] Marzbanrad J, Alijanpour M, Kiasat MS. Design and analysis of an automotive bumper beam in low-speed frontal crashes. Thin-Wall Struct 2009;47:902–11.
[19] Patel NM, Penninger CL, Renaud JE. Topology synthesis of extrusion-based nonlinear transient designs. J Mech Des 2009;191:1–11.
[20] Farkas L, Canadas C, Donders S, van Langenhove T, Tzannetakis N. Optimization study of a parametric vehicle bumper subsystem under multiple load cases using lms virtual lab and optimus. In: 7th European LS-DYNA conference; 2009.
[21] Farkas L, Moens D, Donders S, Vandepitte D. Optimisation study of a vehicle bumper subsystem with fuzzy parameters. Mech Syst Signal Process 2012;32:59–68.
[22] Duponcheele G, Tilley DG. Topological optimization of a bumper beam via the messy genetic algorithm. In: Proceedings of the institution of mechanical engineers; 1998.
[23] Zhang Z, Liu S, Tang Z. Design optimization of cross-sectional configuration of rib-reinforced thin-walled beam. Thin-Wall Struct 2009;47:868–78.
[24] Zarei HR, Kröger M. Bending behavior of empty and foam-filled beams: structural optimization. Int J Impact Eng 2008;35:521–9.
[25] Shin MK, Yi SI, Park GJ. Structural optimization of the automobile frontal structure for pedestrian protection and the low-speed impact test. J Automob Eng 2008;222:2373–87.
[26] Mullerschon Heiner, Lazarov Nikolay, Witowski Katharina. Application of topology optimization for crash with ls opt/topology. In: 11th international LS DYNA users conference; 2010.
[27] Kim SS, Lee KW, Lee DH, Lee HG. Bumper system development to meet new iihs bumper test using cae and optimization. In: SAE World Congress & Exhibition; 2009.
[28] Detwiler DT, Miller RA. Development of a sport utility front bumper system for pedestrian safety and 5 mph impact performance. In: Honda R&D Americas Paper Number 01-S6-W-145.
[29] Lee J-W, Yoon K-H, Kang Y-S, Park G-J. Vehicle hood and bumper structure design to mitigate casualties of pedestrian accidents. In: SAE Paper Number 05-0105.
[30] Park DK, Jang CD. Optimum suv bumper system design considering pedestrian performance. Int J Automot Technol 2010;11/ 6:819–24.
[31] Davoodi MM, Sapuan SM, Yunus R. Conceptual design of a polymer composite automotive bumper energy absorber. Mater Des 2008;29:1447–52.
[32] Ferrer B, Ivorra S, Segovia E, Irles R. Tridimensional modelization of the impact of a vehicle against a metallic parking column at a low speed. Eng Struct 2010;32(8):1986–92.
[33] Karimi Hamid Reza, Pawlus Witold, Robbersmyr Kjell G. Signal reconstruction, modeling and simulation of a vehicle full-scale crash test based on Morlet wavelets. Neurocomputing 2012;93:88–99.
[34] Thanh Le, Itoh Yoshito. Performance of curved steel bridge railings subjected to truck collisions. Eng Struct 2013;54:34–46.
[35] Wang Qian, Fang Hongbing, Li Ning, Weggel David C, Wen Guilin. An efficient {FE} model of slender members for crash analysis of cable barriers. Eng Struct 2013;52:240–56.
[36] Sharma Hrishikesh, Gardoni Paolo, Hurlebaus Stefan. Probabilistic demand model and performance-based fragility estimates for {RC} column subject to vehicle collision. Eng Struct 2014;74:86–95.
[37] Jiga Gabriel, Stamin Stefan, Popovici Dorina, Dinu Gabriela. Study of shock attenuation for impacted safety barriers. Procedia Eng 2014;69:1191–200. 24th {DAAAM} international symposium on intelligent manufacturing and automation, 2013.
[38] Hou Shujuan, Tan Wei, Zheng Yuna, Han Xu, Li Qing. Optimization design of corrugated beam guardrail based on rbf-mq surrogate model and collision safety consideration. Adv Eng Softw 2014;78:28–40.
[39] Fang Howie, Wang Qian, Weggel David C. Crash analysis and evaluation of cable median barriers on sloped medians using an efficient finite element model. Adv Eng Softw 2015;82:1–13.
[40] Willibrordus J. Witteman, Improved vehicle crashworthiness design by control of the energy absorption for different collision situations, Technische Universiteit Eindhoven; 1999.
[41] Frontal impact, <http://www.euroncap.com/tests/frontimpact.aspx>; 2014 [accessed on 11.2014].
[42] Deb A, Naravane A, Chirwa EC. An offset rigid barrier-based test:Equivalence to the insurance institute for highway safety frontal offset impact safety test. Int J Crashworthiness 2006;11(4):281–90.
[43] Liao Xingtao, Li Qing, Yang Xujing, Zhang Weigang, Li Wei. Multiobjective optimization for crash safety design of vehicles using stepwise regression model. Struct Multidiscip Optim 2008;35:561–9.
[44] Jonsen P, Isaksson E, Sundin KG, Oldenburg M. Identification of lumped parameter automotive crash models for bumper system development. Int J Crashworthiness 2009;14(6):533–41.
[45] Pawlus Witold, Reza Hamid, Robbersmyr Kjell Gunnar. Application of viscoelastic hybrid models to vehicle crash simulation. Int J Crashworthiness 2011;16(2):195–205.

[46] Timothy Marler R, Kim Chang-Hwan, Arora Jasbir S. System identification of simplified crash models using multi-objective optimization. Comput Methods Appl Mech Eng 2006;195:4383–95.
[47] Fang H, Solanki K, Horstemeyer MF. Numerical simulations of multiple vehicle crashes and multidisciplinary crashworthiness optimization. Int J Crashworthiness 2010;10(2):161–71.
[48] Finite element model archive, <http://www.ncac.gwu.edu/vml/models.html>; 2014 [accessed 01.2014].
[49] Johnson GR, Cook WH. A constitutive model and data for metals subjected to large strains, high strain rates, and high temperatures. In: Proceedings of the 7th international symposium ballistics; 1983.
[50] Lesuer DR, Kay GJ, LeBlanc MM. Modeling large strain, high rate deformation in metals. In: Modeling the performance of engineering structural materials II. In: Proceedings of a symposium sponsored by the SMD of TMS, Indianapolis, IN; 2001. p. 75–86.
[51] Johnson GR, Cook WH. Fracture characteristics of three metals subjected to various strains, strain sates, temperatures and pressures. Eng Fract Mech 1985;21(1):31–48.
[52] Tanlak N, Sonmez FO, Talay E. Detailed and simplified models of bolted joints under impact loading. J Strain Anal Eng Des 2011;46(3):213–25.
[53] Liuwei G, Jilin Y. Dynamic bending response of double cylindrical tubes filled with aluminum foam. Int J Impact Eng 2011;38:85–94.